Imaging Mass Spectrometry of a Specific Fragment of Mitogen-Activated Protein Kinase/Extracellular Signal-Regulated Kinase Kinase Kinase 2 Discriminates Cancer from Uninvolved Prostate Tissue

Lisa H. Cazares,[1,2,3] Dean Troyer,[1,3] Savvas Mendrinos,[3] Raymond A. Lance,[3,5] Julius O. Nyalwidhe,[1,2,3] Hind A. Beydoun,[4] Mary Ann Clements,[1,2,3] Richard R. Drake,[1,2,3] and O. John Semmes[1,2,3]

Abstract

Purpose: Histopathology is the standard approach for tissue diagnostics and centerpiece of pathology. Although the current system provides prognostic information, there is need for molecular markers that enhance diagnosis and better predict clinical prognosis. The ability to localize disease-specific molecular changes in biopsy tissue would help improve critical pathology decision making. Direct profiling of proteins from tissue using matrix-assisted laser desorption/ionization imaging mass spectrometry has the potential to supplement morphology with underlying molecular detail.

Experimental Design: A discovery set of 11 prostate cancer (PCa)–containing and 10 benign prostate tissue sections was evaluated for protein expression differences. A separate validation set of 54 tissue sections (23 PCa and 31 benign) was used to verify the results. Cryosectioning was done to yield tissue sections analyzed by a pathologist to determine tissue morphology and mirror sections for imaging mass spectrometry. Spectra were acquired and the intensity of signals was plotted as a function of the location within the tissue.

Results: An expression profile was found that discriminates between PCa and normal tissue. The overexpression of a single ion at *m/z* 4,355 was able to discriminate cancer from uninvolved tissue. Tandem mass spectrometry identified this marker as a fragment of mitogen-activated protein kinase/extracellular signal-regulated kinase kinase kinase 2 (MEKK2). The ability of MEKK2 to discriminate tumor from normal cells was orthogonally confirmed.

Conclusions: This study highlights the potential of this approach to uncover molecular detail that can be correlated with pathology decision making. In addition, the identification of MEKK2 shows the ability to discover proteins of relevance to PCa biology. (Clin Cancer Res 2009;15(17):5541–51)

Authors' Affiliations: [1]Department of Microbiology and Molecular Cell Biology, [2]George L. Wright Center for Biomedical Proteomics, [3]The Virginia Prostate Center, and [4]The Graduate Program in Public Health, Eastern Virginia Medical School; [5]Urology of Virginia, Sentara Medical Group, Norfolk, Virginia

Received 11/5/08; revised 5/1/09; accepted 6/2/09; published OnlineFirst 8/18/09.

Grant support: USPHS grant CA085067 from the National Cancer Institute as a part of the Early Detection Research Network (O.J. Semmes).

The costs of publication of this article were defrayed in part by the payment of page charges. This article must therefore be hereby marked *advertisement* in accordance with 18 U.S.C. Section 1734 solely to indicate this fact.

Note: Supplementary data for this article are available at Clinical Cancer Research Online (http://clincancerres.aacrjournals.org/).

Requests for reprints: O. John Semmes, Department of Microbiology and Molecular Cell Biology, Eastern Virginia Medical School, 700 West Olney Road, Norfolk, VA 23507. Phone: 757-446-5904; Fax: 757-446-5766; E-mail: semmesoj@evms.edu.

doi:10.1158/1078-0432.CCR-08-2892

Prostate cancer (PCa) is one of the most common malignancies in the United States (1). It is clinically heterogeneous, with a highly variable natural history (2). The discovery and widespread use of serum prostate-specific antigen (PSA) monitoring for early detection has greatly changed the way PCa is diagnosed and treated. However, PSA lacks specificity as a screening tool for PCa, and there is really no lower limit of PSA that entirely excludes cancer (3). Thus, clinical decision making in PCa places a significant burden on biopsy results. Ultrasound-guided needle biopsy is the standard for diagnosis; however, a negative result does not exclude the presence of cancer. Both sampling and analytic variables account for false-negative results. In practice, false-negative results engender a need for repeat biopsies, which can delay diagnosis and treatment or unnecessarily subject cancer-free men to repeat biopsies and their attendant anxiety and risk (4, 5). The heterogeneity of

Translational Relevance

Prostate cancer (PCa) is a leading cause of death and morbidity in U.S. men. Despite consistent improvement in the management of this disease, there still remain unacceptable sequelae. It is estimated that upwards of 20% of patients with low-risk, clinically organ-confined PCa ultimately progress with biochemical recurrence. In addition, upwards of 10% of men presenting for radical prostatectomy will have insignificant PCa on prostatectomy pathology evaluation. Matrix-assisted laser desorption/ionization imaging mass spectrometry allows for the direct imaging of molecular detail within tissue. Such detail linked with histology could improve decision making about PCa. Our study provides proof of principle that this technique can deliver spatially defined functionally significant molecular detail of patient tissues. We show the ability to reproducibly discriminate tumor from uninvolved tissue. Furthermore, the identification of mitogen-activated protein kinase/extracellular signal-regulated kinase kinase kinase 2 shows that the molecular detail being probed by matrix-assisted laser desorption/ionization imaging mass spectrometry is not limited to traditional high-abundance proteins.

PCa is also a significant problem, as the death rates from PCa are relatively low compared with those from the other major cancers, such as lung, pancreas, and colon. The Gleason grading system, which has been widely adopted for PCa, is a strong predictor of outcome (6). However, a major limitation of this grading system, and a result of aggressive screening procedures, is that most newly diagnosed PCa cases are Gleason grade 6 or 7 tumors. These moderately differentiated tumors can either be indolent or aggressive (7). New methods to assist pathologists in both diagnostic and prognostic decision making are needed to aid in the detection and treatment of PCa.

Matrix-assisted laser desorption/ionization imaging mass spectrometry (MALDI-IMS) of tissue can be used to monitor disease-specific alterations *in situ* at the protein level, both qualitatively and quantitatively (8). This technique, pioneered by Richard Caprioli, holds promise for both the discovery of new molecular markers and the analysis of known markers by examining their expression in tissue and registering output to point of origin within the tissue. MALDI-IMS has the power to link the molecular detail of mass spectrometry with morphology, generating mass spectra correlated to orthogonally characterized locations within a tissue section (9–11). Several recent studies underscore the potential of MALDI-IMS for clinical histopathology applications. Protein expression profiles obtained from tissue could discriminate lung cancer subtype (12). Tumor histology, therapeutic response, and patient survival were shown to correlate with the protein expression patterns obtained from direct tissue analysis in breast tumors (13, 14). Protein expression patterns and images were also found to correlate with brain tumor histology and patient survival (15). Similar discovery efforts using MALDI-IMS have yielded potential candidates in ovarian, colon, and PCa (16–18). However, critical questions remain about the integration of this technique with clinical decision making. In addition, there is concern as to whether the molecular information obtained derives from molecules of biological significance.

To address these questions and to specifically investigate the potential of MALDI-IMS for the diagnosis of PCa, we examined 75 (21 in the initial discovery set and 54 in the validation set) prostate sections for differential expression between tumor and uninvolved tissue. We found that specific protein/peptide expression changes correlated with the presence or absence of PCa. Of particular note, the overexpression of a single peptide at m/z 4,355 was able to accurately define cancer tissue from normal tissue. Tandem mass spectrometry analysis identified this marker as a fragment of mitogen-activated protein kinase (MAPK)/extracellular signal-regulated kinase (ERK) kinase kinase 2 (MEKK2), a member of the MAPK signaling pathway. Immunohistochemistry confirmed that analysis of MEKK2 expression could discriminate tumor from adjacent and distal uninvolved tissues. Our results underscore the potential of MALDI-IMS to discriminate tumor from nontumor tissues and show that MALDI-IMS can reveal biologically significant molecular detail from tissues.

Materials and Methods

Patients and tissue samples. Patients were consented before undergoing radical prostatectomy at Sentara Norfolk General Hospital. Study protocols were approved by the institutional review board at Eastern Virginia Medical School. The age range of the patients was 46 to 82 y, with a mean age of 58.8 y who underwent surgery between 2003 and 2008. A total of 75 patients undergoing radical prostatectomy (21 for the discovery set and 54 for the validation set) were recruited for this study. Two cored specimens were harvested from each prostate immediately after removal of the gland. Each core is divided longitudinally to create mirrored cores; one was fixed and paraffin embedded and the other is embedded in OCT compound (Sakura Finetek USA) and frozen at 80°C. The frozen blocks yielded 41 sections (10 for the discovery set and 31 for the validation set) of benign tissue harvested from prostate tissue distal from the tumor site and 34 sections (11 for the discovery set and 23 for the validation set) of PCa-containing tissue. Of the 23 tumor-containing tissue sections in the validation set, 14 of these sections also harbored benign tissue adjacent to tumor. These were included as "benign adjacent" samples in the validation set. Cryosectioning was done on a Microm HM 505E cryostat at -20°C. A serial cryosection at 7 μm was stained with H&E as a guide and analyzed by a pathologist to determine tissue morphology. Two additional serial sections at 10 μm were mounted on conductive indium-tin oxide–coated glass slides (Bruker Daltonics) and used for MALDI-IMS.

Materials. Acetonitrile, ethanol, high-performance liquid chromatography–grade water, and 3,5-dimethoxy-4-hydroxycinnamic acid (sinapinic acid) were purchased from Sigma Chemical Co. The α-cyano-4-hydroxycinnamic acid (HCCA) was purchased from Bruker Daltonics. Trifluoroacetic acid (TFA) was purchased from Pierce Biotechnology. Rabbit monoclonal antibody to MEKK2 (EP626Y) was purchased from Abcam.

Tissue section preparation. Immediately after sectioning, the indium-tin oxide–coated slides were washed and fixed with 70% ethanol and 95% ethanol for 30 s each (19). A water wash was done to remove residual embedding medium followed by a repeat of the ethanol washes of 70% and 95%. Slides were air dried and stored in a dessicator for 1 h before matrix deposition. A matrix solution of sinapinic acid (10 mg/mL) containing 75% acetonitrile and 0.13% TFA was sprayed uniformly over the tissue using an automated spraying device (ImagePrep workstation, Bruker Daltonics), which controls matrix deposition

Table 1. Characteristics of patient cohort

Characteristic	Discovery	Validation
PCa tissues		
Patients	11	23
Mean age (range)	59.4 (46-65)	58.5 (46-82)
Mean preoperative PSA, ng/mL (range)	7.97 (4.0-13.3)	11.1 (2.4-69.6)
Pathologic classification		
pT2a	0	3
pT2b	0	1
pT2c	7	8
pT3a	4	8
pT3b	0	3
Gleason score (section tested)		
3+3	9	9
3+4	2	10
4+3	0	4
Total patients/total sections tested	11/11	23/23
Benign tissues		
Patients	10	31
Mean age (range)	58.4 (51-65)	58.8 (46-76)
Mean preoperative PSA, ng/mL (range)	8.30 (4.8-15.5)	10.8 (3.6-51.8)
Pathologic classification		
pT2a	1	4
pT2b	1	1
pT2c	5	8
pT3a	3	12
pT3b	0	6
Total patients/total sections tested	10/10	31/31
Total patients	21	54
Total tissue sections	21	54
Peptides differentially expressed		
	Highly expressed in PCa cells	
	m/z	*P*
	3,373	2.81 E-08
	3,443	7.59 E-09
	3,488	4.38 E-08
	4,027	1.27 E-07
	4,355	2.76 E-16
	Highly expressed in benign cells	
	m/z	*P*
	4,274	7.94 E-021
Correct classification	Discovery set	Validation set
PCa areas	85%	81%

and thickness of the matrix layer. Digital images of the sprayed tissue sections were acquired with a flatbed scanner before MALDI analysis.

MALDI-IMS analysis and image processing. Spectra were collected across the entire tissue area using the Ultraflex III MALDI-TOF/TOF instrument (Bruker Daltonics) with a SmartBeam laser operating at 200 Hz in linear mode over a mass range of m/z 2,000 to 45,000. A laser spot diameter of 100 μm and a raster width of 200 μm were used. Using the FlexImaging software (Bruker Daltonics), teaching points were generated to ensure the correct positioning of the laser for spectral acquisition. The software exports the specific geometry of the tissue to be analyzed, and an instrument-specific automated method is created, which generates a grid across the tissue of spots where the laser will acquire data. A total of 200 laser shots were accumulated and averaged from each laser spot rastered across the tissue section. Calibration was done externally using a peptide standard in the mass range of m/z 700 to 4,500. The intensity of each signal over the entire mass range acquired is plotted as a function of location on the tissue, allowing the visualization of the location of each *m/z* detected. These images were generated and visualized using FlexImaging and BioMap software.[6]

Data processing and statistical analysis. Automated analysis of the spectral data was done to identify all differentially expressed peaks between cell types. Spectra derived from pathology-defined regions of interest (ROI) in each tissue were exported using the FlexImaging software for profile analysis. Baseline subtraction, normalization (to total ion current), peak detection, and spectral alignment were done using ClinProt Tools (Bruker Daltonics). A mass window of 0.3% and a signal to noise ratio of 3 were selected for peak detection. A genetic algorithm using k-nearest neighbors was used to obtain a classification between normal and PCa-containing tissue. The result of the genetic algorithm is the peak combination, which is proved to separate best between the different classes. Significant differences between groups were determined by Student's *t* test. A *P* value of <0.01 was considered to indicate statistical significance. The predictive power of the putative biomarker to detect PCa tissue areas was tested using the area under the receiver operator characteristic (ROC) curve using SAS 9.1 Statistical Software (SAS Institute Cary, NC). The optimal cutoff point was defined as that point on the ROC curve that maximizes both sensitivity and specificity.

Tissue and cell culture lysates. Tissue lysates were prepared from bulk frozen prostate tissue (~0.5 mm^3) by homogenizing the samples in a small Dounce tube on ice with a solution of 20 mmol/L HEPES and 1% Triton X-100 (1 mL). Lysates were then sonicated at room temperature for 15 min and spun down at 14,000 rpm for 2 min to remove cellular debris. The lysates were then subjected to fractionation using weak cationic exchanger magnetic beads (Bruker Daltonics) according to the supplier's specifications. The bound peptides and proteins were eluted in 20 μL. Five microliters of this eluate were lyophilized and resuspended in 5 μL of HCCA matrix in 50% acetonitrile with 0.1% TFA. Lysates from the PCa cell lines (Du145, LNCaP, and PC-3) were prepared from 10^6 cells in a lysis buffer containing 0.3% SDS, 3% DTT, and 30 mmol/L Tris (pH 7.5).

MALDI-MS/MS and protein identification. One microliter of each tissue lysate mixed with matrix was then spotted on a steel MALDI target. The mass profiles were recorded by MALDI-MS using the same acquisition parameters as for tissue imaging. Data were collected on the UltraFlex III in reflectron mode to verify the presence of the peak of interest. MS/MS analysis of the peak was then done in LIFT mode. An optimized high-mass LIFT method was used and externally calibrated with fragments from a peptide standard with parent masses in the mass range of 700 to 4,500 Da. A parent mass was selected and LIFT analysis (MS/MS) was done in the Ultraflex TOF-TOF. Peaks were labeled using FlexAnalysis software supplemented by manual picking using two criteria; peaks displayed a signal to noise of 3 and present in two of three spectral groups. A composite peak list was compiled, and database search was done using MASCOT 2.2.03 with the following settings: MS Tol. of 50 ppm, MS/MS Tol. of 1.3 Da, no enzyme designation, and serine acetylation, using the National Center for Biotechnology Information database for human sequences with 20,080,125 entries.

Trypsin digestion was done on the tissue slices (10 μm) by spotting 0.5 μL of a solution of 0.769 μg/μL trypsin in 50 mmol/L ammonium bicarbonate (pH. 8.0). The tissue slices were then incubated at 37°C for 2 h in a humidity chamber. Following trypsin treatment, the tissue sections were spray coated with HCCA (7 mg/mL in 50% acetonitrile, 0.2% TFA). Data were collected across the tissue in reflectron mode and converted to BioMap images.

Immunohistochemistry. Immunostaining of frozen specimens was done by the avidin-biotin peroxidase complex method using a Vectastain Elite ABC kit (Vector Laboratories). Briefly, frozen tissues were incubated in 0.3% hydrogen peroxide to block endogenous peroxide activity for 15 min. Sections were then exposed to normal goat serum to block nonspecific binding, and endogenous avidin and biotin was blocked with an avidin-biotin blocking kit (Vector Laboratories).

[6] Available as free software from http://www.MALDI-MSI.org.

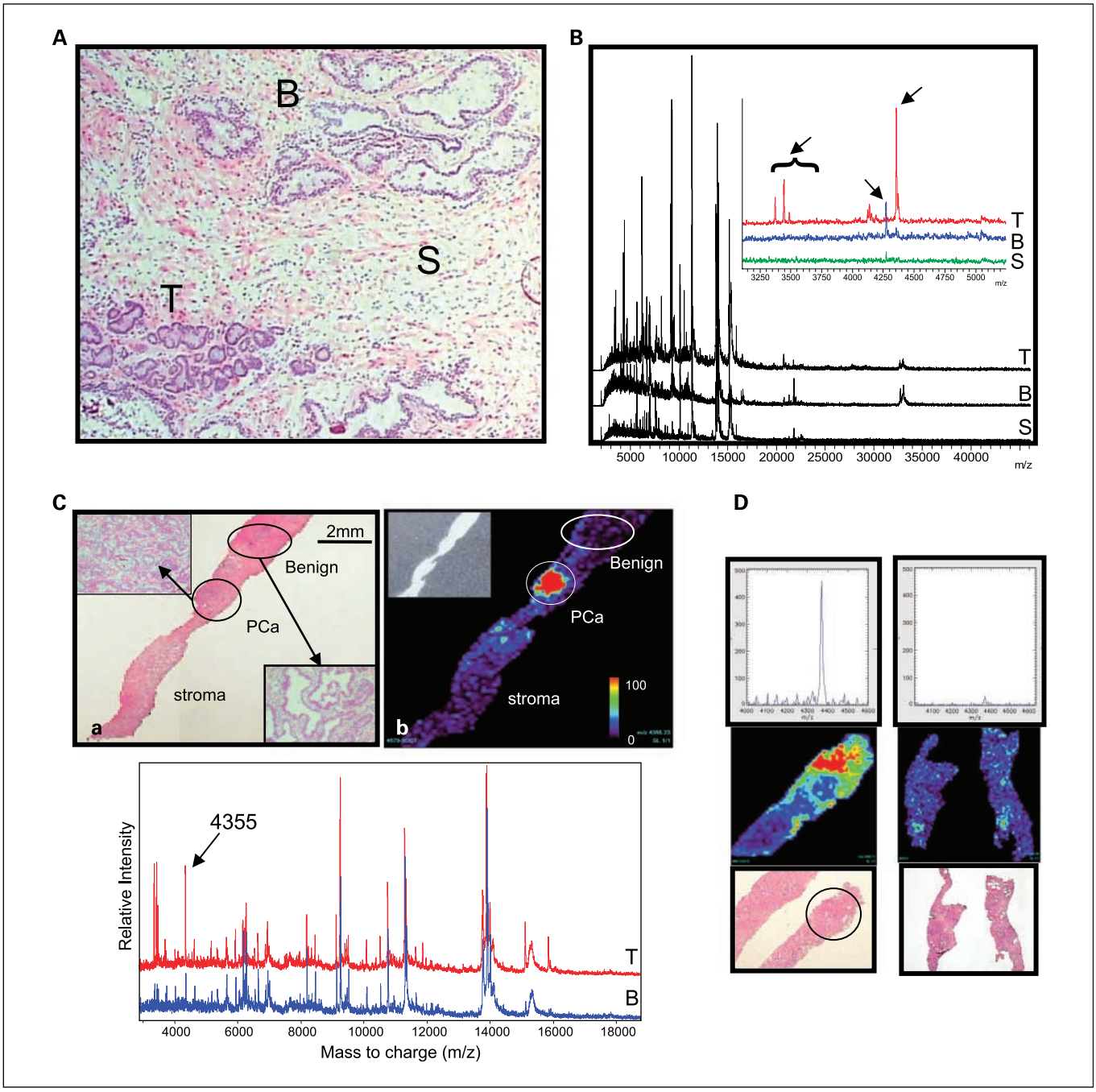

Fig. 1. Direct tissue mass spectrometric analysis of human prostate tissue reveals cell-specific profiles. Frozen prostate tissue was subjected to MALDI-IMS as described. *A,* representative histologic image of H&E-stained prostate tissue showing areas of prostate adenocarcinoma (*T*), benign prostate glands (*B*), and benign stroma (*S*). *B,* resulting average spectra acquired from each region showing characteristic profiles for different cell types. Inset, expanded view of the mass range *m/z* 3,000 to 5,300 showing differences in the profiles for each cell type. *C,* MALDI-IMS of a single prostate tissue containing tumor and uninvolved regions. *a,* H&E image of a tissue specimen containing a defined area of PCa glands and benign glands. Insets, magnified (×10) views of each cell type. *b,* resulting two-dimensional ion density map showing high expression of a peak at *m/z* 4,355 (*red*) in the PCa area (inset is a scan of the tissue after matrix deposition). *c,* average spectra from a single spot obtained in the PCa (*T*) region and from the benign adjacent glandular (*B*) area displaying differential expression of the ion at *m/z* 4,355. *D,* MALDI-IMS two-dimensional ion density maps of a PCa-containing tissue and a benign prostate tissue. Circled, pathology-defined regions of PCa. Areas in red from the resulting MALDI-IMS indicate high expression of *m/z* 4,355. Top, spectra exported from representative regions of each tissue are shown in the *m/z* range of 4,000 to 4,600 and display the *m/z* 4,355 peak profile.

Tissue sections were then incubated with rabbit monoclonal antibody to MEKK2 (EP626Y; Abcam) diluted 1:50 in PBS for 1 h at room temperature. Sections were then treated with biotinylated goat anti-rabbit immunoglobulin G (IgG), followed by treatment with avidin-biotin-peroxidase complex, and stained with IMPACT 3,3′-diaminobenzidine peroxidase substrate (Vector Laboratories) according to the supplier's protocol. Counterstaining was done with Gill's hematoxylin.

Western blot analysis. A total of 30 μg (for cell lysates) or 100 μg (for tissue lysates) of protein were separated on a 4% to 12% SDS-PAGE gel and transferred by semidry transfer method to Immobilon-P membranes (Millipore). The membranes were then incubated in Odyssey

blocking buffer diluted 1:1 in PBS for 1 h at room temperature. Incubation with rabbit monoclonal antibody to MEKK2 diluted 1:1,000 in blocking buffer (PBS, 0.1% Tween 20, 0.01% SDS) was done overnight at 4 °C with gentle shaking. Blots were then washed four times in PBS and 0.1% Tween 20 (PBST). The secondary antibody, Alexa Fluor IRDye 800 CW goat anti-rabbit IgG (LI-COR Biosciences), was diluted 1:5,000 with blocking buffer. The membrane was incubated in secondary antibody solution with shaking at room temperature for 1 h protected from light. The membranes were then washed four times in PBST, rinsed in PBS, and scanned with the Odyssey IR imaging system (LI-COR Biosciences).

Results

Identification of an expression profile that discriminates between PCa and adjacent normal tissue. Our investigation into the presence of a PCa-specific protein/peptide expression profile was conducted on tissue sections from 75 prostates harvested from individuals undergoing radical prostatectomy. The patient and tissue sample characteristics of the discovery and validation cohort are presented in Table 1. Tissue sections were uniformly coated with matrix solution using an automated spraying device, and adjacent serial sections were stained with H&E for histopathology. Parallel-stained slides of each section were read by a genitourinary-trained pathologist, and the ROIs were designated. These ROIs contained prostate adenocarcinoma cell populations, benign epithelial cells, stromal cells, and benign epithelial cells adjacent to tumor cells.

In the initial discovery experiment, we analyzed 21 tissue sections (11 PCa and 10 benign). The resulting spectra were used to generate two-dimensional molecular maps of the peptides and proteins present in each tissue section, and automated analysis of the spectral data was done to identify differentially expressed peaks. The resolving power of our technique was comparable with laser capture microdissection capture of cells followed by MALDI-TOF analysis of the extracted proteins (Supplementary Fig. S1). On average, we could resolve between 350 and 400 peaks within the mass range m/z 2,000 to 20,000. Several peptide ions were found to discriminate PCa from benign tissue (Table 1). Examination by a pathologist reveals specific regions with designated cell types present in prostate tissue sections (Fig. 1A). This process is defined as pathology-designated ROI. In the mass range m/z 3,000 to 5,000, several differentially expressed ions were detected, which could be used to discriminate between PCa and adjacent benign regions (Fig. 1B, *inset*; Table 1). Of particular note are two peptide ions at an average m/z of 4,027 and 4,355, which showed significant overexpression in PCa cells when compared with benign adjacent cell spectra. Another peak at m/z 4,274 was expressed in benign adjacent epithelial cells and stroma with little or no expression seen in PCa cells. Spectra derived from ROIs designated as tumor or benign from the initial 21 tissues examined were used to generate a classification algorithm using three m/z values (m/z 4,027, 4,274, and 4,355), which was capable of correctly classifying 85% of PCa tissue areas. Selected component ions with significant discriminating power were evaluated in these initial tissues and images derived around the pathology-designated ROI. This allowed for a visual determination of region-specific changes in peptide ion expression. Representative examples of images derived from mapping all three discriminating m/z are shown in Supplementary Fig. S2.

The classification ability of the same genetic algorithm derived from the discovery set using the three discriminatory peaks (m/z 4,027, 4,274, and 4,355) was then evaluated on the larger validation set. This set consisted of 23 tumor sections and 31 benign sections for a total of 54 sections (54 cancer-confirmed patients). The performance of the three-peak genetic algorithm in the validation set was comparable with that seen in the discovery set. Specifically, the PCa areas in the validation set could be correctly classified in 81% of the tissues tested (Table 1).

MALDI-IMS using m/z 4,355 can identify PCa-specific regions of prostate. When we examined the list of differentially expressed peaks from our initial discovery set of 21 tissues, the ion at m/z 4,355 was the most significantly overexpressed in PCa-containing tissue regions ($P = 2.76 \times 10^{-16}$). We therefore wanted to evaluate the utility of this peak alone for the detection of PCa regions within prostate tissue via MALDI-IMS. Figure 1C is a representative image of a tissue section with one specific region of PCa and clearly defined adjacent regions of normal prostate glands. A higher magnification view of each cell type can be seen in the insets. Clearly evident from the ion density map, the m/z 4,355 peak was highly expressed in the PCa region compared with the surrounding tissue. Little to no expression is visible in the normal stroma or benign glandular regions. When representative spectra were exported from the specific regions (tumor versus benign), we can clearly observe a prominent peak at m/z 4,355 overexpressed in the PCa-obtained profile.

MALDI-IMS using m/z 4,355 discriminates between cancer and uninvolved prostate tissue. To evaluate the differential expression of m/z 4,355 between PCa and benign regions, we conducted an analysis of the validation set of prostate tissues. We examined the images produced from the ion density of the m/z 4,355 peak following the analysis of 23 PCa and 31 benign prostate tissue sections (distal from tumor site). We also examined an additional 14 benign prostate tissue regions found adjacent to tumor in 14 of the 23 PCa sections used for the validation set. Shown in Fig. 1D are representative ion images of the expression of the m/z 4,355 peak in tissues containing PCa and distal benign sections. The corresponding spectra in the representative region of m/z 4,000 to 4,600 are shown in the top panels above each image. A set value for the peak intensity threshold used to display the m/z 4,355 peak in each image was determined from the discovery set and applied to the validation set. This threshold represented the maximum peak intensity observed from the normalized intensity values obtained in PCa regions. Any pixel displaying an intensity greater than or equal to this set threshold was then considered high expression and is represented in the images obtained in the validation set. An intensity scale can be seen at the bottom right of Fig. 1C. We provide in Supplementary Fig. S3 a representative set of eight paired tissues. High expression was visible in each section, where PCa cells were present or visible throughout the tissue when no benign cells were present. In contrast, little to no expression of the m/z 4,355 ion was detected in sections containing benign cells only.

To illustrate the tissue-specific expression of m/z 4,355, we examined the intensity values with respect to defined tissue regions across the separate validation sample set. Intensity values for m/z 4,355, normalized to total ion current, were calculated

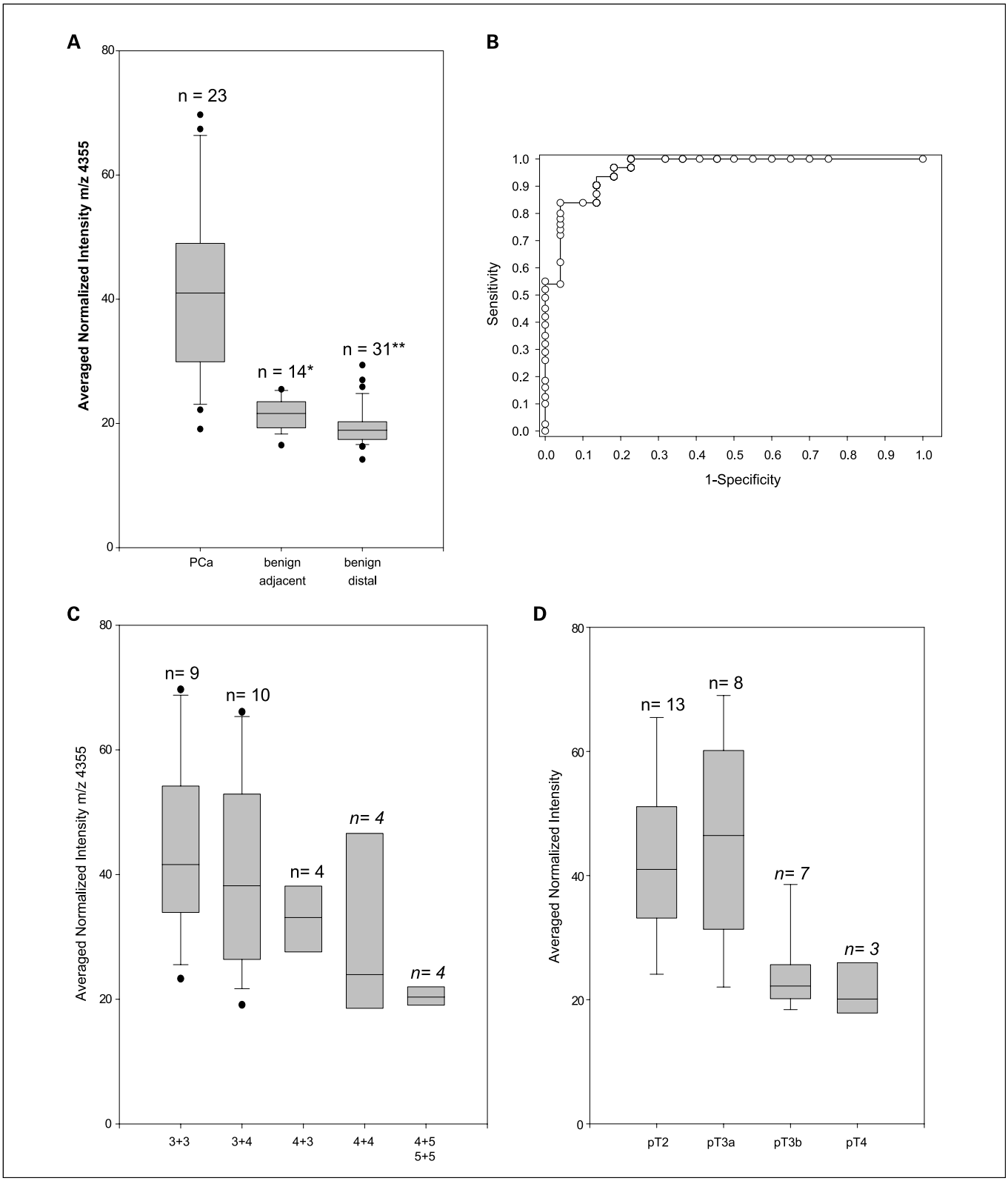

Fig. 2. The normalized intensity values for *m/z* 4,355 can discriminate tumor from benign tissue. *A,* normalized average intensity values for *m/z* 4,355 in different prostate tissue areas. A total of 23 PCa-containing tissues, 14 benign adjacent, and 31 distal benign tissues were analyzed via MALDI-IMS. The resulting normalized average intensity values for the *m/z* 4,355 peak were plotted for PCa, benign adjacent, and benign distal regions. The boundary of the box closest to zero indicates the 25th percentile, a line within the box marks the median, and the boundary of the box farthest from zero indicates the 75th percentile. Whiskers above and below the box indicate the 90th and 10th percentiles. *, $P = 3.2$ E-5; **, $P = 4.0$ E-10. *B,* the predictive power of the putative biomarker to detect PCa tissue areas was tested using the area under the ROC curve. Averaged normalized intensity values obtained from MALDI-IMS spectra for PCa tissue were plotted according to Gleason grade (*C*) or pathologic stage (*D*). The high-grade samples [$n = 8$: from tissues with grade 4+4 ($n = 4$) and 4+5 ($n = 4$)] with pathologic stage pT3b ($n = 5$) or pT4 ($n = 3$) are included in the plots but were not part of the validation set.

for each tissue region and plotted: PCa, benign adjacent, and benign distal (Fig. 2A). The average normalized intensity of the *m/z* 4,355 peak in benign tissue found in the same section with PCa cells or benign prostate tissue from a section containing no PCa cells was 20.8 and 19.6, respectively, whereas for PCa regions the average intensity found was 41.1, representing a 2.1-fold increase. A ROC curve calculated from the average normalized intensity of each ROI (distal benign versus PCa) is shown in Fig. 2B. The optimal cutoff point for using the 4,355 peak as a biomarker for PCa in tissue sections was a normalized average intensity value of 33. This cutoff point was associated with a sensitivity of 90.3% and a specificity of 86.4% (area under curve AUC 0.960). To maximize sensitivity, a cutoff value of 23.8 was chosen, which represents a sensitivity of 96.8% and a specificity of 81.8%.

We next conducted a more detailed analysis of the expression of the *m/z* 4,355 by disease stage/grade. We plotted the normalized intensity values for *m/z* 4,355 by Gleason grade and pathologic stage. The results of this analysis can be seen in Fig. 2C and D. Tissues with a Gleason combined score of 3+3 had an averaged normalized intensity value for *m/z* 4,355 of 44.8, with 89% of the tissues exhibiting a value above the ROC cutoff of 23.8. Tissues with a Gleason score of 3+4 had an averaged normalized intensity value of 41.0, with 90% of these tissues displaying a value above the ROC cutoff. Tissues with a Gleason score of 4+3 had an averaged normalized intensity of 32.0, with

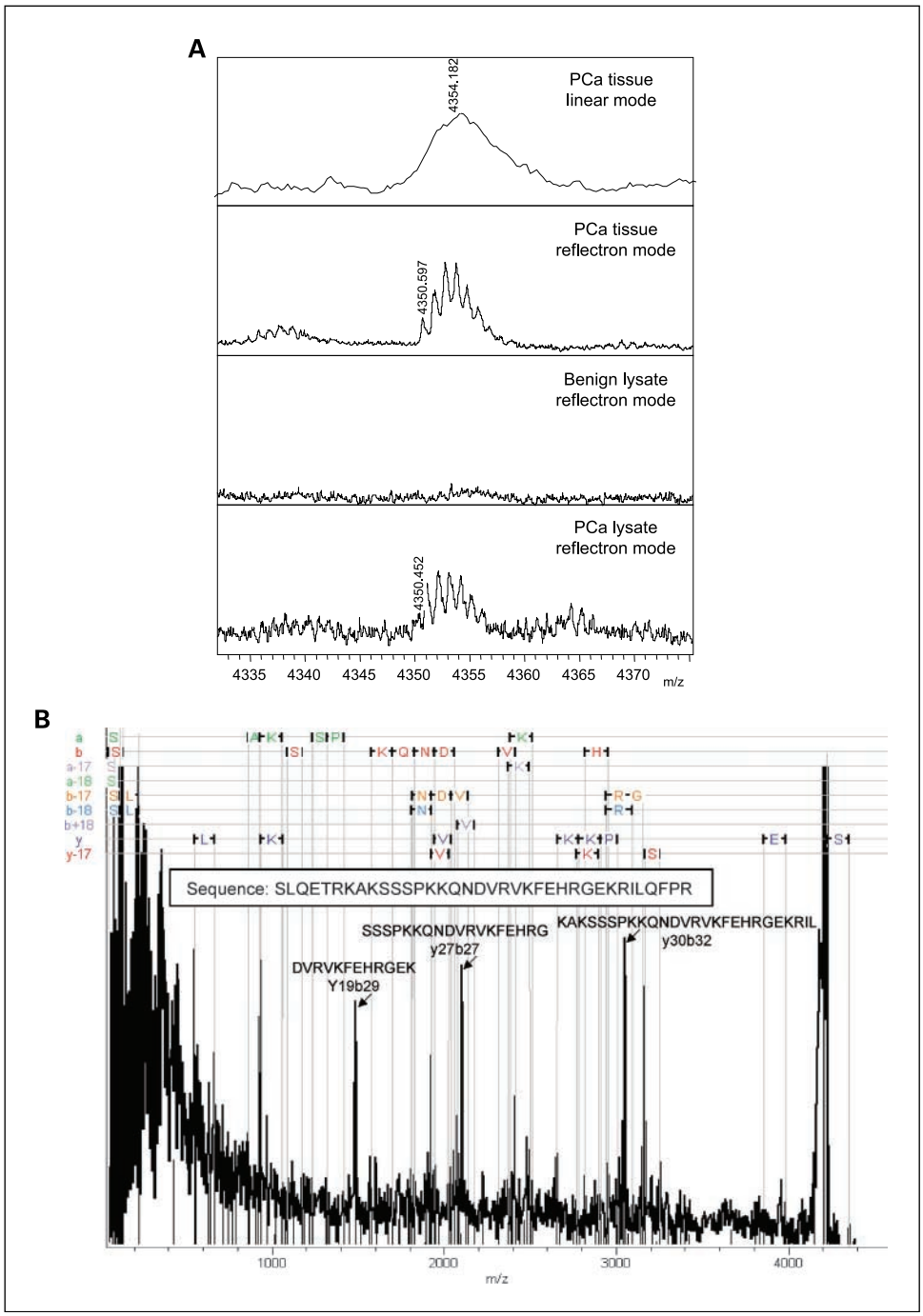

Fig. 3. Sequence identification of the peptide at *m/z* 4,355. *A,* spectra showing the peak profile of *m/z* 4,355 collected by direct acquisition from tissue or from tissue lysates as indicated in each panel in linear or reflectron mode. *B,* deconvoluted MS/MS spectra of monoisotopic peak (*m/z* 4,350.4) collected using TOF/TOF LIFT. Peaks attributed to internal fragments are labeled and indicated with arrows.

75% of tissues displaying a value above the ROC cutoff. This reduction in expression of the *m/z* 4,355 peak observed with increasing Gleason grade was also observed between pathologic stage. Although this reduction was not significant between Gleason scores, a significant reduction was seen between pathologic stages pT2 and pT3b as well as pT3a versus pT3b. Tissues from prostates designated as pT2a, pT2b, or pT2c had a normalized average intensity of 42.7, with 92.3% of the tissue samples above the cutoff. A similar trend is seen in tissues from prostates designated pT3a, which had an average intensity of 45.6 for *m/z* 4,355, with 87.5% of the tissues with a value above 23.8. If, however, the tissue specimen was procured from a prostate with a pathologic designation of pT3b indicating seminal vesicle invasion, the average normalized intensity dropped to 30.1, with only 28.6% of tissues having a value above the cutoff.

To further define the trend of decreasing expression of 4,355 with increasing stage/grade of disease, we examined an additional eight sections from more aggressive disease (Gleason 8/9/10 and pT4). The analysis was conducted as described above for the previous tissues, and the evaluation of 4,355 was conducted with the same cutoff score. As can be seen in Fig. 2C and D, the trend toward decreased expression was observed in higher grade/stage disease. Specifically, of the eight high-grade tissues tested, only two (25%) had expression above the cutoff value of 23.8. Of the high-grade cases, three were designated as pT4 and only one (33%) of these had a normalized intensity value for *m/z* 4,355 above the cutoff.

Sequence identification of m/z 4,355 as a fragment of MEKK2. Having established the differential expression of a peptide ion at *m/z* 4,355, we next set out to sequence identify the peptide. Lysates were prepared from four tissue samples: two PCa and two benign prostate. Sections from these tissues were examined in the initial MALDI-IMS analysis and found to have high or low expression of the peak at *m/z* 4,355. Protein lysates were incubated with weak cationic magnetic beads, and eluted fractions were shown to be enriched for the *m/z* 4,355 peak as measured by MALDI-TOF. As seen in Fig. 3A, the peptide ion captured from the weak cationic exchanger fractionation of the PCa tissue lysate matches the mass detected directly from the tissue within an error of 0.26 Da, whereas no peptide ion was detected at this *m/z* in the enriched lysate from benign tissue. The lysate was then concentrated via lyophilization and prepared for MS/MS analysis as described. Figure 3B is a representative MS/MS spectra showing the fragmentation pattern of the parent ion (*m/z* 4350.4), in which several large internal fragments are observable. The composite fragmentation series gave a MASCOT top score of 42.3 (1.3 Da, 50 ppm), with scores ≥37 indicating significant homology, and matched to a fragment of MEKK2 (Swiss-Prot entry Q9Y2U5) with S-acetylation at the NH_2 terminus of the peptide (Supplementary Fig. S2). Of 84 total observed peaks, 79 could be accurately assigned to theoretical fragments of MEKK2. This sequence represents amino acid residues 26 to 61 in the 619–amino acid full-length protein and lies within the PhoX-and-Bem1 (PB1) domain of the molecule.

To further establish that the *m/z* 4,355 ion derived from tissue is a fragment of MEKK2, we did an in-tissue digest to analyze for the presence of predicted MEKK2 tryptic fragments. A tissue section previously found to have high expression of the *m/z* 4,355 peak in a PCa region was used for this analysis. Serial sections of the same tissue region were harvested and analyzed. One of the mirror sections was trypsin treated, whereas the adjacent mirror section

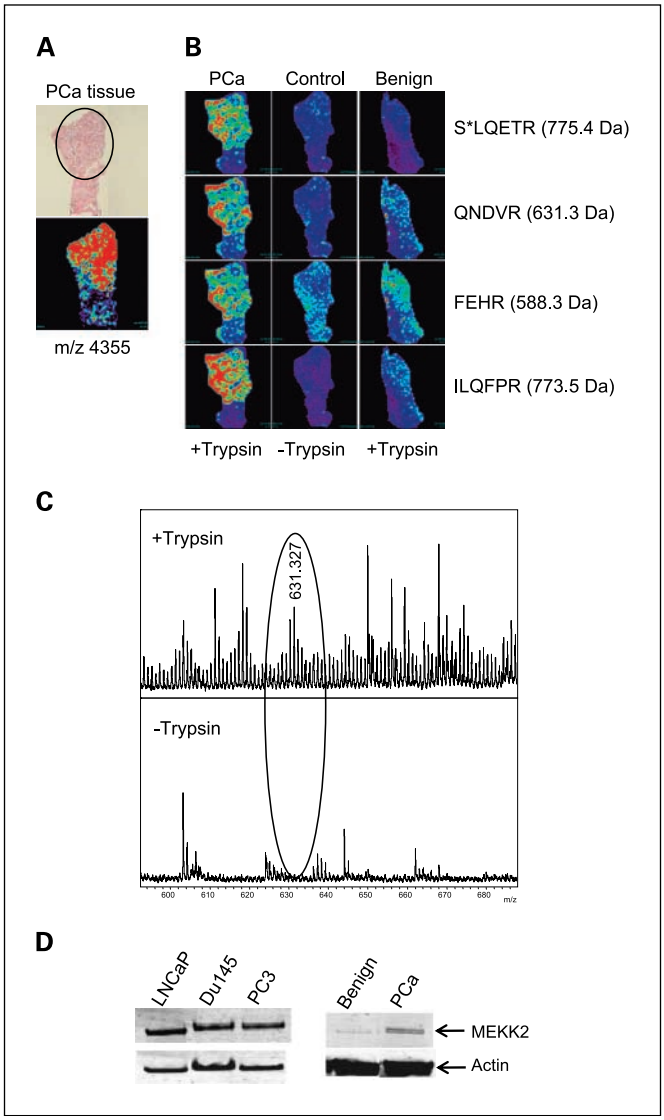

Fig. 4. On-tissue trypsin digestion of PCa region detects predicted peptides of MEKK2 fragment. *A,* H&E-stained image of PCa tissue with a region of adenocarcinoma circled (*top*) and MALDI-IMS showing spatial distribution of parent ion at *m/z* 4,355 (*bottom*). *B,* after trypsin treatment of the same tissue, four predicted fragments corresponding to the MEKK2 fragment sequence (**SLQETR**KAKSSSPKK**QNDVRV**K**FEHR**GEKR**ILQFPR** fragments detected are in bold) were detected in the PCa tissue. Control is a serial section of PCa tissue without trypsin treatment. A benign section of prostate tissue was also trypsin treated. *C,* representative spectra from trypsinized (*top*) and nontrypsinized (*bottom*) PCa tissue showing the presence of an ion at *m/z* 631.3 in the trypsin-treated tissue only. *D,* Western blot analysis for expression of MEKK2 in the indicated PCa cell lines and tissue lysates. Western blot of PCa cell lines (30 μg) and tissue lysates (100 μg) was done using an antibody to the NH_2-terminal region of MEKK2. Actin was used as a loading control.

was untreated and used as a control. Ion density maps were also generated using the indicated theoretical tryptic peptides. As seen in Fig. 4, specific theoretical masses of the predicted MEKK2 fragments after trypsinization could be detected in the trypsin-treated PCa tissue. The in-tissue trypsin-generated fragments matching the theoretical digest masses were not present in the mirror untreated section of the same PCa tissue (Fig. 4C). Furthermore, trypsin digestion of benign tissue sections did not generate observable fragment ions corresponding to theoretical MEKK2 cleavage products (Fig. 4B). We also show a representative ion density map

image derived from the parental *m/z* 4,355 as a comparison with images derived from the tryptic peptides (Fig. 4A). This analysis shows that both the parental peptide and predicted peptide fragments display concordant tissue expression.

Expression of MEKK2 in PCa cell lines and tissues. Western blot analysis was done on PCa and benign tissue extracts and three PCa cell lines (Du145, LNCaP, and PC-3). LNCaP cells originate from a lymph node metastatic lesion of human PCa, and Du145 and PC-3 are human prostate adenocarcinoma cell lines metastatic to the brain and bone, respectively. The relative expression of MEKK2 in these systems is shown in Fig. 4D. All three prostate cell lines showed strong expression of full-length MEKK2 (70 kDa). This analysis revealed higher MEKK2 expression in the PCa tissues when compared with the expression seen in the benign tissues. Densitometry analysis indicated a 4.4-fold increased expression of MEKK2 in PCa tissue compared with benign tissue.

MEKK2 is overexpressed in PCa-specific regions of the prostate. In some cases, the overexpression of a fragment of a protein may coincide with overexpression of the whole protein. If this is the case, then selective overexpression of MEKK2 in tissue would be further confirmation of our results. We examined the expression of MEKK2 in PCa tissue using immunohistochemistry. PCa-containing and uninvolved frozen tissues were stained for MEKK2 expression. The antibody used is specific for the NH_2-terminal portion of the MEKK2 protein where the PB1 domain is located and is the same one used above for the Western blot analysis (20). As seen in Fig. 5A, MEKK2 staining correlates with the presence of PCa in the tissue section. The ROI designated in the H&E panel was prescribed by a genitourinary-specialized pathologist as containing tumor. Additional prostate tissues were also stained, and magnified views of the stained PCa glands and benign tissue can be seen in Fig. 5B. In Fig. 5C, we show an analysis of sections designated as all tumor or all benign. The prostate tissues examined showed high levels of MEKK2 within involved tissue with predominantly cytoplasmic expression pattern. In contrast, benign glands displayed little to no MEKK2 expression.

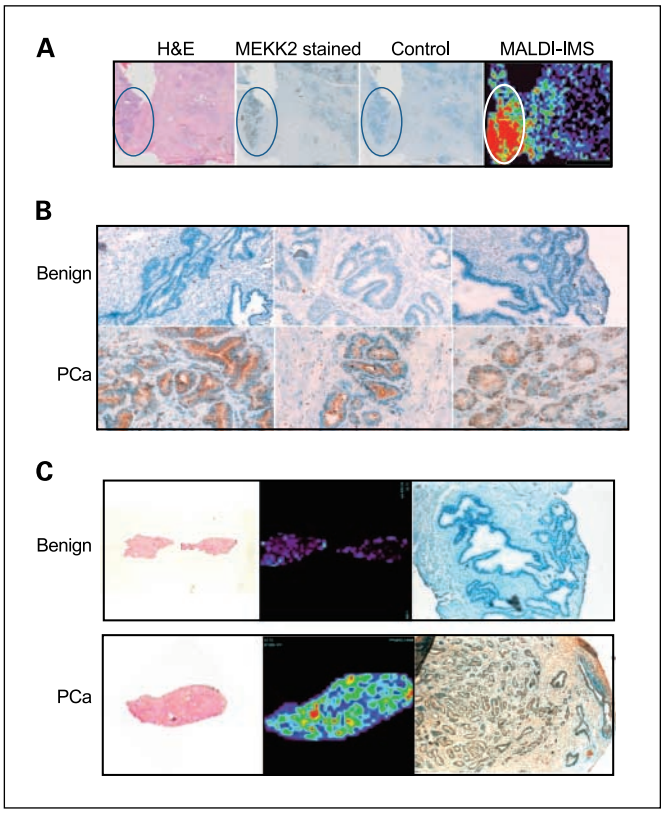

Fig. 5. MEKK2 expression in prostate tissue. *A,* immunohistochemical analysis of frozen prostate tissue sections. H&E-stained prostate tissue with a region of PCa circled (*left*), MEKK2-stained serial section showing staining in PCa regions (*middle left*), and control section without primary antibody (*middle right*). MALDI-IMS two-dimensional ion density map for *m/z* 4,355 indicating high expression in the region of PCa, which stained for MEKK2. *B,* representative areas of MEKK2 staining from three benign (magnification, ×100) and three PCa tissues (magnification, ×200) showing strong expression of MEKK2 in adenocarcinoma cells and little expression in benign glands. *C,* MEKK2 immunostaining corresponding to *m/z* 4,355 MALDI-IMS expression in two tissue samples. H&E-stained serial sections (*left*) are shown for benign (*top*) and PCa tissue (*bottom*) with the corresponding MALDI-IMS two-dimensional ion density maps indicating *m/z* 4,355 expression (*middle*). Right, MEKK2 immunostaining. Magnification, ×50.

Discussion

The correlation of molecular information to histopathologic structures offers tremendous potential for improved characterization of clinical tissues. The use of MALDI-IMS and profiling to obtain such molecular information in the form of protein and peptide distributions greatly enhances the ability to identify potential candidates for new specific biomarkers. In their groundbreaking study, Yanagisawa et al. (12) showed that *m/z* patterns obtained directly from lung tissue could be used to classify histologic groups and predict nodal involvement and survival in non–small cell lung cancer. Similar results were obtained for ovarian cancer in which peptide profiling by direct MALDI analysis of 25 ovary carcinomas (stages III and IV) and 23 benign tissues identified several peptides observed to only be present in carcinoma compared with benign samples (21). The most prevalent peptide was identified as a fragment of immunoproteasome PA28. Specific to PCa, MALDI-IMS revealed a specific expression pattern that was temporally associated with prostate development in an animal model (22), and in a separate study, a pattern of *m/z* was associated with pathogenesis of PCa in a cohort of 22 prostate tissue samples (17). In our current study, we used MALDI-IMS in an attempt to discriminate tumor from uninvolved prostate tissues. Unique to our study design was the use of a large tissue set that allows for a discovery group (11 PCa/10 uninvolved) and a separate test/validation group (23 PCa/31 uninvolved) for examining the performance of the selected biomarker. The performance of a single biomarker was associated with the corresponding image in which PCa tissue could be detected. We also sequence identify the *m/z* generating peptide as a fragment of MEKK2 and confirmed the differential expression of MEKK2 between tumor and benign tissue using immunohistochemistry and Western blot.

Biochemical and genetic studies have shown that MAP3Ks are crucial in relaying distinct cell surface signals through various downstream MAPK pathways. MEKK2 is 1 of only 2 of the 20 known MAP3Ks, the other being MEKK3, which regulate the MEK5/ERK5 pathway (23–25). Growth factors and oxidative/osmotic stress have been shown to stimulate the three-tier ERK5 kinase module consisting of MEKK2/3, MEK5, and ERK5. MEKK2 and MEKK3 encode PB1 domains that selectively heterodimerize with the MEK5 PB1 domain to form a functional MEKK2 (or MEKK3)-MEK5-ERK5 ternary complex

(23, 25). The ERK5 pathway mediates normal cell-cell interactions during immune surveillance and is a critical regulator of cell invasion during tumor metastasis (reviewed in ref. 26). Indeed, the ERK5 pathway has been implicated in high-grade PCa. Specifically, an increase in MEK5 expression was associated with metastatic PCa, cell proliferation, matrix metalloproteinase-9 expression, and cell invasion (27). Strong MEK5 expression was also found to correlate with the presence of bony metastases and less favorable disease-specific survival. An additional report found significant correlation between ERK5 cytoplasmic overexpression, Gleason sum score, and less favorable disease-specific survival (28). The authors also found that ERK5 nuclear expression is significantly associated with the transition from hormone-sensitive to hormone-refractory disease. Clearly, our finding that MEKK2 is overexpressed in tumor compared with benign is consistent with established biological behavior of ERK5 signaling.

One study, examining the interactions of the MEK5 PB1 domain, found that both MEKK2 and ERK5 interact with the NH_2-terminal extension of MEK5, suggesting that MEKK2 and ERK5 compete for binding to MEK5 rather than form a ternary complex (29). The PB1s are dimerization/oligomerization domains that are present in adaptor and scaffold proteins as well as kinases. PB1 domain–dependent MEKK2/3-MEK5 heterodimers provide a spatially organized signaling complex primed to activate ERK5 in response to activation of MEKK2 or MEKK3. No other MAPK cascade has been shown to form such a complex. Interestingly, the *m/z* 4,355 peak represents a peptide fragment that lies within the PB1 domain and may reflect molecular pathway changes indicative of PCa development.

Clearly, the utility of a tissue-assessed biomarker, such as MEKK2, is restricted to decisions made in pathology using biopsy or surgical material. The specific utility of a tumor-confined biomarker in PCa is limited, unless the expression varies with disease stage or prognosis. Our observation that the expression of the MEKK2 4,355 peptide is reduced in higher stage/grade disease (G = 4+3, pT3b) needs to be verified in a larger cohort with representation of more aggressive disease. In addition, such studies should include an assessment of the expression of MEKK2 with respect to observable disease outcome or surrogate clinical end points. We are particularly interested in determining if MEKK2 expression correlates with the presence of insignificant disease. In addition, differing thresholds for atypical lesions, assessment of Gleason score, and diagnosis of small cancers are known sources of analytic variability. In fact, second-opinion reviews suggest that reclassification of a malignant to benign lesion occurs in 1% to 2% of cases, and in up to 10% of cases, a change in Gleason score affecting clinical decision making may occur (30, 31). Thus, MEKK2 may provide for better staging/grading with potentially improved diagnostic uniformity.

Although our results show that MALDI-IMS can be a powerful biomarker discovery tool, in order for MALDI-IMS to be clinically useful it must contribute to the ability of pathologists and surgeons to make accurate diagnosis and prognosis. One attractive feature of the MALDI-IMS is the ability to display protein expression and spatial distribution as an intensity map, thus allowing for visual integration into the diagnostic workflow. However, the integration of MALDI-IMS into clinical diagnostics will ultimately depend on the competitive advantage over existing methods for assessing tissue biomarkers. Here, we specifically refer to immunohistochemistry of formalin-fixed tissues. Although immunohistochemistry is widely applied, and used with great success, it is helpful to remind ourselves of the limitations of immunohistochemistry. When conditions are fully optimized, semiquantitation using an appropriate chromogenic detection system can be achieved. Morphometry and densitometry can also be used to correlate signal with histology. However, it is important to realize that the resulting signal is "secondary" to the analyte and displays quantitation on par with a Western blot. In fact, high-throughput immunohistochemistry as practiced in a clinical pathology laboratory is usually optimized to produce a "strong" signal using the best antigen retrieval technique. Thus, optimization implies "visible" and quantitation implies relative quantitation. The variables of the antigen retrieval process and antibody-based detection methods are therefore intrinsic to the way tissues are fixed and processed. The need for antibody-antigen–specific optimization makes it impractical to routinely use multivariate immunohistochemistry. Another disadvantage of immunohistochemistry is that it is notoriously difficult to raise antibodies to specific posttranslational modifications, short peptides, and subtle protein structural isoforms that may be of relevance to regulation of cellular signaling pathways. Alternatives should be explored, as the demands for precision and accuracy in our diagnostics will only increase as the number of targeted agents increases.

Imaging mass spectrometry has the potential to address some of the shortcomings of immunohistochemistry. For instance, because IMS directly measures the analyte, it is possible to obtain direct quantitation and the platform is amenable to multiplexed analysis. In addition, IMS can readily determine posttranslational modifications of proteins potentially providing information not obtained by indirect measurements. The ability to quantitate small amounts of intact or modified proteins becomes especially crucial in situations where small core biopsies of tumors are done, and clinical decision making begins before definitive excision when larger portions of tumors become available. In counterbalance to these advantages, there are several practical obstacles for the clinical application of IMS. Most prominent perhaps is that although MALDI-IMS on paraffin-embedded, formalin-fixed samples has been done (16), such efforts have met with limited success. Thus, the development and use of alternative fixatives is a critical area of investigation (32). We are currently investigating alternative fixation methods, including the commercially available UMFix approach developed at the University of Miami (33).

Our studies presented here highlight the potential for MALDI-IMS to be integrated into clinical decision making. Clearly, the specific utility of the *m/z* 4,355 generated by a peptide of MEKK2 will need to be established through future studies involving direct assessment of biopsy tissue and pathology outcome. However, our immunohistochemical analysis shows that MEKK2 is overexpressed in tumor-involved tissues within the prostate. Although ERK5 has been shown to correlate with high-grade disease, this is the first demonstration of MEKK2 overexpression in prostate tumors and potential correlation with cancer stage/grade. We are currently examining the role of MEKK2 activation in respect to ERK5 activity and tumor progression. Overall, our findings suggest that application of MALDI-IMS to identify disease-specific molecular changes in tissue will provide molecular detail to improve the critical pathology decision-making process in PCa diagnosis.

Disclosure of Potential Conflicts of Interest

No potential conflicts of interest were disclosed.

References

1. Hayat MJ, Howlader N, Reichman ME, Edwards BK. Cancer statistics, trends, and multiple primary cancer analyses from the Surveillance, Epidemiology, and End Results (SEER) Program. Oncologist 2007;12:20–37.
2. Nelen V. Epidemiology of prostate cancer. Recent Results Cancer Res 2007;175:1–8.
3. Thompson IM, Pauler DK, Goodman PJ, et al. Prevalence of prostate cancer among men with a prostate-specific antigen level < or = 4.0 ng per milliliter[see comment][erratum appears in N Engl J Med. 2004 Sep 30;351(14):1470]. N Engl J Med 2004;350:2239–46.
4. Djavan B, Remzi M, Schulman CC, Marberger M, Zlotta AR. Repeat prostate biopsy: who, how and when? A review. Eur Urol 2002;42:93–103.
5. Epstein JI, Herawi M. Prostate needle biopsies containing prostatic intraepithelial neoplasia or atypical foci suspicious for carcinoma: implications for patient care. J Urol 2006;175:820–34.
6. Egevad L, Granfors T, Karlberg L, Bergh A, Stattin P. Prognostic value of the Gleason score in prostate cancer. BJU Int 2002;89:538–42.
7. Pinthus JH, Witkos M, Fleshner NE, et al. Prostate cancers scored as Gleason 6 on prostate biopsy are frequently Gleason 7 tumors at radical prostatectomy: implication on outcome. J Urol 2006;176:979–84, discussion 84.
8. Caprioli RM, Farmer TB, Gile J. Molecular imaging of biological samples: localization of peptides and proteins using MALDI-TOF MS. Anal Chem 1997;69:4751–60.
9. Chaurand P, Cornett DS, Caprioli RM. Molecular imaging of thin mammalian tissue sections by mass spectrometry. Curr Opin Biotechnol 2006; 17:431–6.
10. Caldwell RL, Caprioli RM. Tissue profiling by mass spectrometry: a review of methodology and applications. Mol Cell Proteomics 2005;4: 394–401.
11. Chaurand P, Sanders ME, Jensen RA, Caprioli RM. Proteomics in diagnostic pathology: profiling and imaging proteins directly in tissue sections. Am J Pathol 2004;165:1057–68.
12. Yanagisawa K, Shyr Y, Xu BJ, et al. Proteomic patterns of tumour subsets in non-small-cell lung cancer. Lancet 2003;362:433–9.
13. Cornett DS, Mobley JA, Dias EC, et al. A novel histology-directed strategy for MALDI-MS tissue profiling that improves throughput and cellular specificity in human breast cancer. Mol Cell Proteomics 2006;5:1975–83.
14. Reyzer ML, Caldwell RL, Dugger TC, et al. Early changes in protein expression detected by mass spectrometry predict tumor response to molecular therapeutics. Cancer Res 2004;64:9093–100.
15. Schwartz SA, Weil RJ, Thompson RC, et al. Proteomic-based prognosis of brain tumor patients using direct-tissue matrix-assisted laser desorption ionization mass spectrometry. Cancer Res 2005;65:7674–81.
16. Lemaire R, Desmons A, Tabet JC, Day R, Salzet M, Fournier I. Direct analysis and MALDI imaging of formalin-fixed, paraffin-embedded tissue sections. J Proteome Res 2007;6:1295–305.
17. Schwamborn K, Krieg RC, Reska M, Jakse G, Knuechel R, Wellmann A. Identifying prostate carcinoma by MALDI-imaging. Int J Mol Med 2007;20:155–9.
18. Shimma S, Sugiura Y, Hayasaka T, Hoshikawa Y, Noda T, Setou M. MALDI-based imaging mass spectrometry revealed abnormal distribution of phospholipids in colon cancer liver metastasis. J Chromatogr B Analyt Technol Biomed Life Sci 2007.
19. Goodwin RJ, Dungworth JC, Cobb SR, Pitt AR. Time-dependent evolution of tissue markers by MALDI-MS imaging. Proteomics 2008;8:3801–8.
20. Fanger GR, Johnson NL, Johnson GL. MEK kinases are regulated by EGF and selectively interact with Rac/Cdc42. EMBO J 1997;16:4961–72.
21. Lemaire R, Menguellet SA, Stauber J, et al. Specific MALDI imaging and profiling for biomarker hunting and validation: fragment of the 11S proteasome activator complex, Reg α fragment, is a new potential ovary cancer biomarker. J Proteome Res 2007;6:4127–34.
22. Chaurand P, Rahman MA, Hunt T, et al. Monitoring mouse prostate development by profiling and imaging mass spectrometry. Mol Cell Proteomics 2008;7:411–23.
23. Nakamura K, Johnson GL. PB1 domains of MEKK2 and MEKK3 interact with the MEK5 PB1 domain for activation of the ERK5 pathway. J Biol Chem 2003;278:36989–92.
24. Uhlik MT, Abell AN, Cuevas BD, Nakamura K, Johnson GL. Wiring diagrams of MAPK regulation by MEKK1, 2, and 3. Biochem Cell Biol 2004;82:658–63.
25. Nakamura K, Uhlik MT, Johnson NL, Hahn KM, Johnson GL. PB1 domain-dependent signaling complex is required for extracellular signal-regulated kinase 5 activation. Mol Cell Biol 2006;26:2065–79.
26. Van den Steen PE, Dubois B, Nelissen I, Rudd PM, Dwek RA, Opdenakker G. Biochemistry and molecular biology of gelatinase B or matrix metalloproteinase-9 (MMP-9). Crit Rev Biochem Mol Biol 2002;37:375–536.
27. Mehta PB, Jenkins BL, McCarthy L, et al. MEK5 overexpression is associated with metastatic prostate cancer, and stimulates proliferation, MMP-9 expression and invasion. Oncogene 2003;22:1381–9.
28. McCracken SR, Ramsay A, Heer R, et al. Aberrant expression of extracellular signal-regulated kinase 5 in human prostate cancer. Oncogene 2008;27:2978–88.
29. Seyfried J, Wang X, Kharebava G, Tournier C. A novel mitogen-activated protein kinase docking site in the N terminus of MEK5α organizes the components of the extracellular signal-regulated kinase 5 signaling pathway. Mol Cell Biol 2005;25:9820–8.
30. Chan TY, Epstein JI. Patient and urologist driven second opinion of prostate needle biopsies. J Urol 2005;174:1390–4, discussion 4; author reply 4.
31. Nguyen PL, Schultz D, Renshaw AA, et al. The impact of pathology review on treatment recommendations for patients with adenocarcinoma of the prostate. Urol Oncol 2004;22:295–9.
32. Chaurand P, Latham JC, Lane KB, et al. Imaging mass spectrometry of intact proteins from alcohol-preserved tissue specimens: bypassing formalin fixation. J Proteome Res 2008;7:3543–55.
33. Vincek V, Nassiri M, Nadji M, Morales AR. A tissue fixative that protects macromolecules (DNA, RNA, and protein) and histomorphology in clinical samples. Lab Invest 2003;83: 1427–35.